Improving the axial and lateral resolution of three-dimensional fluorescence microscopy using random speckle illuminations

Awoke Negash,[1] Simon Labouesse,[1] Nicolas Sandeau,[1] Marc Allain,[1] Hugues Giovannini,[1]
Jérôme Idier,[2] Rainer Heintzmann,[3] Patrick C. Chaumet,[1] Kamal Belkebir,[1] and Anne Sentenac[1,*]

[1]Aix Marseille Université, CNRS, Centrale Marseille, Institut Fresnel, UMR 7249, 13013 Marseille, France
[2]IRCCYN, CNRS, UMR 6597, 44321 Nantes, France
[3]Institute of Physical Chemistry and Abbe Center of Photonics, Friedrich Schiller University Jena, 07743 Jena, Germany
*Corresponding author: anne.sentenac@fresnel.fr

We consider a fluorescence microscope in which several three-dimensional images of a sample are recorded for different speckle illuminations. We show, on synthetic data, that by summing the positive deconvolution of each speckle image, one obtains a sample reconstruction with axial and transverse resolutions that compare favorably to that of an ideal confocal microscope.   © 2016 Optical Society of America

1. INTRODUCTION

Improving the resolution and contrast of three-dimensional images of fluorescent samples while conserving the ease of use and noninvasiveness of classical microscopy is a major challenge. Classical brightfield microscopes, in which the fluorescence is excited by a homogeneous intensity, exhibit, in the best case, a lateral resolution about half the emitted wavelength with an axial resolution three times bigger [1]. In addition, due to the specific shape of the optical transfer function, it is plagued by an important out-of-focus signal coming from the low-frequency sample structures which deteriorates significantly the image contrast.

Optical sectioning techniques, such as confocal microscopy, light sheet microscopy [2], and others [3,4], ameliorate the image contrast but give little resolution improvement over brightfield. In contrast, structured illumination microscopy (SIM) improves both the image contrast and the transverse and axial resolutions [5], but it requires careful control of the three-dimensional excitation pattern which is not always possible in thick samples.

In this paper, we present a technique that provides optical sectioning and transverse and axial resolution improvement without requiring control of the illuminations. Our approach is inspired from the blind structured illumination microscopy technique developed in Refs. [6–8] in simplified bidimensional configurations. It consists of recording several images of the sample for different speckles and processing the data with an appropriate reconstruction algorithm that does not require

knowledge of the illuminations. We demonstrate this approach on synthetic data, mimicking that of standard fluorescence microscopes.

2. RECONSTRUCTION ALGORITHMS

In the three-dimensional (3D) blind-SIM approach, the sample is illuminated with L different 3D intensity patterns I_l, $l = 1, \ldots, L$. For each illumination, a 3D fluorescence image of the sample M_l is recorded. To keep the illumination unchanged, the scanning along the optical axis should be done by remote focusing [9] or by using a specific device that projects on the camera, within one shot, several images taken at different focal planes [10]. Under these experimental conditions, the recorded 3D data, $M_l(\mathbf{r}_{n=1,\ldots,N})$, where $\mathbf{r}_{n=1,\ldots,N}$ are the centers of the N voxels forming the investigated volume, can be modeled as in Ref. [5] as

$$M_l(\mathbf{r}_n) = [(\rho I_l) * h](\mathbf{r}_n) + \epsilon, \qquad (1)$$

where ρ is the sample fluorescence density, h is the three-dimensional point spread function of the microscope, ϵ is the experimental noise, and $*$ stands for the convolution operator. For the sake of simplicity, Eq. (1) is rewritten using notations of operators as

$$M_l = \mathbf{A}(\rho I_l) + \epsilon, \qquad (2)$$

where the linear operator $\mathbf{A}$ describes the convolution of Eq. (1). The issue is to estimate ρ from the L images $M_{l=1,\ldots,L}$ obtained under different speckle realizations $I_{l=1,\ldots,L}$

and to obtain a better reconstruction than that given by the deconvolution of a 3D brightfield microscope image.

Different inversion techniques able to produce high-resolution sample reconstructions from low-resolution speckle images have been proposed in the two-dimensional blind-SIM configuration. They can be fundamentally distinguished by the way the sample is represented, either as a set of single emitters [7,8] or as a continuously varying fluorescence density [6,12]. In this work, we were inspired by the latter approach, in agreement with the modeling of the data given by Eq. (1).

We have first adapted to the three-dimensional configuration the blind-SIM inversion algorithm presented in Ref. [6]. This inversion technique, hereafter denoted as blind-SIM simultaneous inversion (blind-SIM-SI), consists of estimating simultaneously the sample ρ and the illuminations $I_{l=1,...,L}$ so as to minimize a cost functional indicating the mismatch between the data and the model. Since all the details are provided in Ref. [6], we only recall the main points of the approach. First, the number of unknowns is lessened using the *a priori* information that the sum of the illuminations is homogeneous. This assumption is generally verified in classical structured illumination schemes and applies if enough speckle realizations are considered. The homogeneity constraint is introduced in the inversion scheme by writing I_L as $I_0 - \sum_{l=1}^{L-1} I_l$, where I_0 is a constant over the whole 3D image. In addition, both ρ and $I_{l=1,...,L-1}$ are considered positive and written with auxiliary variables as $\rho = \xi^2$ and $I_l = i_l^2$ [6]. Then the simultaneous estimations of ρ and $I_{l=1,...,L-1}$ are obtained by minimizing the cost functional,

$$F(\xi, i_{l=1,...,L-1}) = W \sum_{l=1}^{L} \sum_{n=1}^{N} \|M_l(\mathbf{r}_n) - \mathbf{A}(\xi^2 i_l^2)\|^2, \quad \textbf{(3)}$$

where $W = 1/(\sum_{l=1}^{L} \sum_{n=1}^{N} \|M_l(\mathbf{r}_n)\|^2)$. The minimization is performed with a classical conjugate gradient algorithm. All the details about this algorithm are provided in the supplementary methods of Ref. [6].

In a second study, aimed at accelerating the inversion procedure, we derived a simpler reconstruction scheme, hereafter denoted as blind-SIM separate deconvolution (blind-SIM-SD), that does not reconstruct explicitly the illuminations. Introducing the auxiliary variable $q_l = \rho I_l$ for $l = 1, ..., L$, the blind-SIM problem can be stated as finding q_l positive so as to minimize

$$H(q_{l=1,...,L}) = W \sum_{l=1}^{L} \sum_{n=1}^{N} \|M_l(\mathbf{r}_n) - \mathbf{A}(q_l)\|^2. \quad \textbf{(4)}$$

Once the q_l are known, the indetermination on ρ and I_l is removed by using the homogeneity constraint on the illuminations $\sum_{l=1}^{L} I_l = I_0$ to form $\rho = (\sum_{l=1}^{L} q_l)/I_0$. The minimization of H can be done by deconvolving separately each speckle image under the positivity constraint which fastens remarkably the inversion procedure. In this work, we use an original deconvolution technique which is straightforwardly adapted from the previous blind-SIM-SI algorithm. We write $q_l = \eta_l^2$ and estimate η_l by minimizing

$$G(\eta_l) = W_l \sum_{n=1}^{N} \|M_l(\mathbf{r}_n) - \mathbf{A}(\eta_l^2)\|^2, \quad \textbf{(5)}$$

where $W_l = 1/(\sum_{n=1}^{N} \|M_l(\mathbf{r}_n)\|^2)$. As for the previous algorithm, the minimization is performed with a conjugate gradient technique (more details are provided in Appendix A).

Comparing the cost functional F, Eq. (3), to G, Eq. (5), and bearing in mind the homogeneity constraint, one observes that the two reconstruction schemes are basically solving the same problem. The main difference is that, in the first approach, the Lth intensity, written as $I_0 - \sum_{l=1}^{L-1} I_l$, is not positive, while, in the second approach, all the intensities are positive. The equal treatment of all the speckle intensities and the rapidity of the minimization of G compared to that of F are strong assets in favor of the second scheme. However, when the illuminations are partially known, as in classical SIM with distorted illuminations, blind-SIM-SI remains a better option as it can easily incorporate *a priori* information on the illumination patterns [11,12] contrary to blind-SIM-SD.
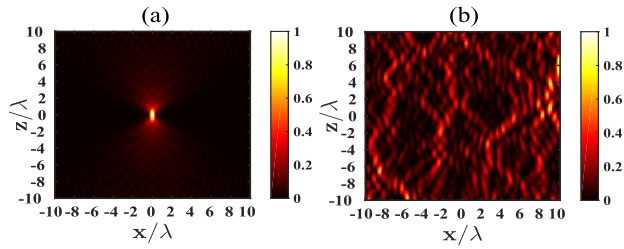
3. ANALYSIS OF THE OPTICAL SECTIONING AND RESOLUTION IMPROVEMENT OF BLIND SIM

In this section, we investigate the performances of the blind-SIM approach on synthetic data stemming from various samples. The blind-SIM 3D reconstructions are compared to the positive deconvolutions of "standard" brightfield and confocal images. The brightfield image is obtained by summing all the speckle images, which ensures that the comparison is performed with the same photon budget. The ideal confocal image (obtained with an infinitely small pinhole) is simulated by convolving the actual fluorescence distribution of the sample with the square of the point spread function h^2 [13] and deteriorating it with Poisson noise using the same photon budget as the other techniques. In both cases, the positive deconvolution is performed with the same algorithm as that used in blind-SIM-SD. It is worth noting that the confocal image is unrealistic as it combines the use of an infinitely small pinhole with a large number of collected photons. Actually, it should rather be considered as an indication of the ultimate resolution that can possibly be achieved using structured illumination than as a feasible experiment.

In all the following numerical experiments, we consider a microscope objective with NA = 0.95 and $\lambda = 550$ nm, where λ is the excitation and fluorescence wavelength. The voxel size of the image is $\lambda/(8\text{NA})$ in all directions. To be realistic from an experimental point of view, only one hundred different speckles were considered to generate the data. Note that with this limited number of illuminations, the speckle average exhibits a non-negligible inhomogeneity. Except for the last simulation, we considered data with an average global photon budget per pixel of about 10^6 so that Poisson noise is negligible.

The speckle and the point spread function of the microscope, displayed in Figs. 1(a) and 1(b), are modeled using a simple scalar model. Noting the space variable $\mathbf{r} = \mathbf{r}_\parallel + z\hat{\mathbf{z}}$, where $\hat{\mathbf{z}}$ indicates the optical axis, the speckle is approximated by

$$I_l(\mathbf{r}) = \left| \int_D e^{i\phi_l(\mathbf{k}_\parallel)} e^{i\sqrt{k_0^2 - k_\parallel^2} z} e^{i\mathbf{k}_\parallel \cdot \mathbf{r}_\parallel} d\mathbf{k}_\parallel \right|^2, \quad \textbf{(6)}$$

Fig. 1. (a) Cut in the $y = 0$ plane of the normalized point spread function, and (b) the normalized speckle intensity.

where $k_0 = 2\pi/\lambda$ is the illumination wavenumber, $\phi_l(\mathbf{k}_\parallel)$ is an uncorrelated random variable uniformly distributed between 0 and 2π, and D is a disk of radius NAk_0. The point spread function is given by

$$h(\mathbf{r}) = C \left| \int_D e^{i\sqrt{k_0^2 - k_\parallel^2} z} e^{i\mathbf{k}_\parallel \cdot \mathbf{r}_\parallel} \mathrm{d}\mathbf{k}_\parallel \right|^2, \qquad (7)$$

where C ensures that $\int h(\mathbf{r})\mathrm{d}\mathbf{r} = 1$.

In a first example, we consider a thin fluorescent star-like sample in the $y = 0$ plane whose fluorescence density is defined by

$$\rho(x, y, z) \propto [1 + \cos(30\theta)]\delta(y), \qquad (8)$$

where $\tan\theta = z/x$; see Fig. 2(a). This kind of target permits an easy visualization of the resolution improvement as its spatial frequencies increase as one gets closer to the star center. To get an idea about the data being processed, we display in Fig. 2(b) an image of the sample obtained under one speckle illumination.

In Figs. 2(c) and 2(d), the brightfield image and its deconvolution are shown. As expected, the image resolution is not isotropic, in contrast to that obtained with the same sample placed in the $(x–y)$ transverse plane [6]. The lack of resolution for the quasi-horizontal sample features is the signature of the tore-shaped support of the microscope optical transfer function $\hat{h}$ [13]. The grainy aspect of the reconstruction stems from the residual inhomogeneity of the speckle average which is clearly visible in Fig. 2(c).

The reconstructions obtained with blind-SIM-SI and blind-SIM-SD are given in Figs. 2(g) and 2(h), respectively. Apart from the presence of some hot spots in Fig. 2(g) which deteriorates slightly the image rendering, both reconstructions exhibit similar performances. The transverse and axial resolutions are significantly better than that of the brightfield image and comparable to that of the ideal confocal image, Figs. 2(e) and 2(f). These observations, which have been confirmed by many other examples (not shown), leads to two important comments.

First, when there is no *a priori* information on the illuminations except the homogeneity of their sum, blind-SIM-SD is a much better option than blind-SIM-SI as it is faster and less prone to the apparition of hot spots. Hereafter, all the blind-SIM reconstructions will be performed with the blind-SIM-SD algorithm.

Second, the blind-SIM-SD scheme corresponding to a simple positive deconvolution of each speckle image implies that the recovery of sample frequencies beyond the optical transfer function cutoff can only be explained by the positivity constraint
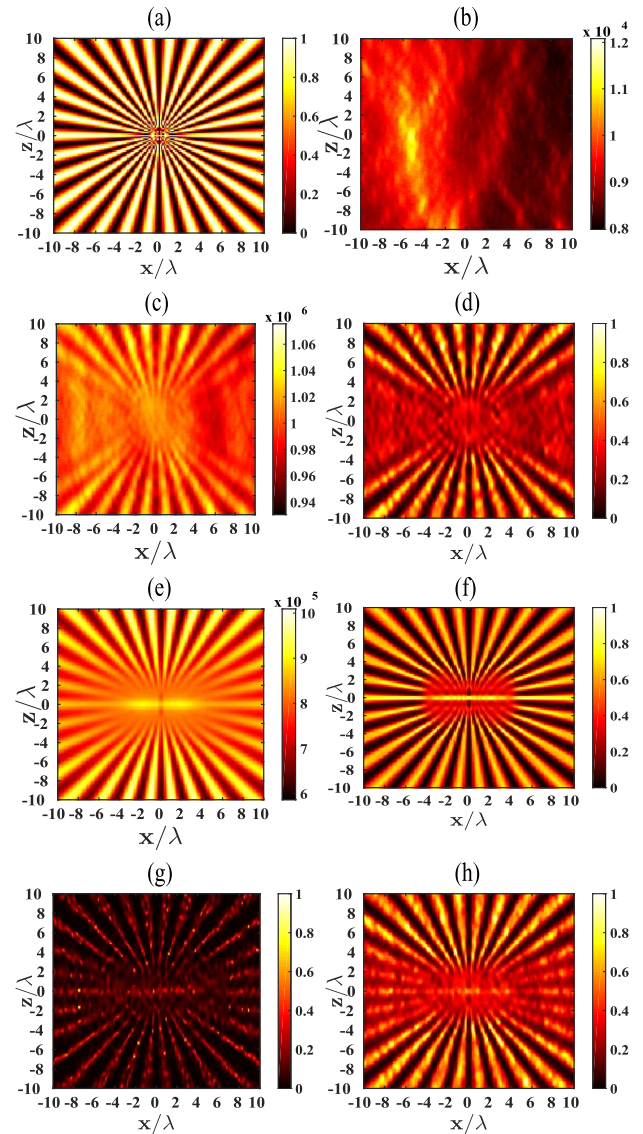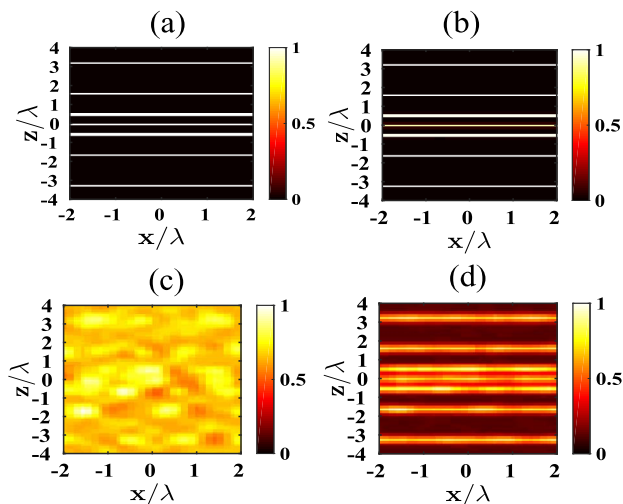

Fig. 2. Reconstructions of a thin fluorescent $(x–z)$ plane with an oscillating radial fluorescence distribution (star-type sample). The sample is illuminated by 100 different speckles. (a) Fluorescence density of the sample. (b) Example of one intensity image obtained for a given speckle illumination. (c) Brightfield image of the sample obtained by summing the 100 speckles images. (d) Positive deconvolution of the brightfield image (c). (e) Image of an ideal confocal microscope. (f) Positive deconvolution of the confocal image (e). (g) Reconstruction with the blind-SIM-SI algorithm. (h) Reconstruction with the blind-SIM-SD algorithm. In (b), (c), and (e), the colorbar indicates the number of recorded photons. In (a), (d), and (f)–(h), the colorbar indicates the normalized fluorescence density.

[14]. The better resolution of blind-SIM-SD reconstruction compared to the positive deconvolution of the brightfield data stems from the more frequent activation of the positivity constraint on the speckle images than on the brightfield one. Yet, it is observed that the recovery of the sample high spatial frequencies remains limited to the sample spectrum participating in the image formation Eq. (1). In our case, with speckle generated with the same objective as the point spread function,
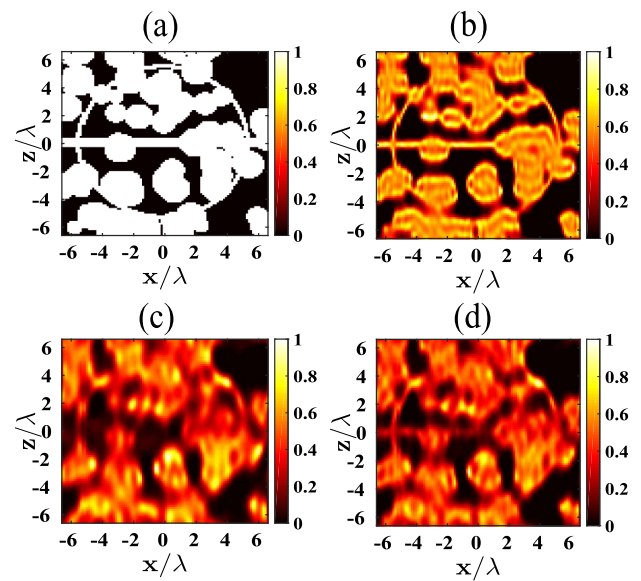
the speckle images depend on the sample spectrum within the support of h^2. This property can explain the similarity between the blind-SIM and confocal images.

In Fig. 3, we investigate more specifically the optical sectioning ability of blind-SIM-SD by considering a sample made of thin fluorescent transverse planes placed at various z. As in the previous experiment, the sample is illuminated by 100 different speckles. A cut of the sample is depicted in Fig. 3(a). In this example, the sample spatial frequencies are located along the z axis only. Since the optical transfer function of fluorescence microscopy removes all the sample spatial frequencies but 0 along the z axis, the theoretical brightfield image of fluorescent (x–y) planes is a constant in the whole volume and so is its deconvolution. In our experiment, the speckle average being still inhomogeneous, the deconvolution of the brightfield image, Fig. 3(c), is not a constant but the fluorescent planes positions are not visible. In contrast, the reconstruction obtained with blind-SIM-SD permits us to distinguish the fluorescent planes [Fig. 3(d)] with an accuracy approaching that of the confocal deconvolved image [Fig. 3(b)]. Note that the spectacular accuracy of the deconvolved confocal image is attributable to the positivity constraint which is particularly efficient on sparse samples [14].

Last, in Figs. 4 and 5 we study a more complex three-dimensional sample made of beads inside and outside two halves of a big sphere. This specific geometry was chosen to investigate the performance of the imaging technique for surface-like objects (such as membranes) and volumic objects. Cuts of the sample in the $y = 2.6\lambda$ and $z = -1.6\lambda$ planes are displayed in Figs. 4(a) and 5(a), respectively. The deconvolved confocal and brightfield images and the blind-SIM-SD reconstruction in the two planes are shown in Figs. 4(b)–4(d) and Figs. 5(b)–5(d), respectively. These results confirm the interest
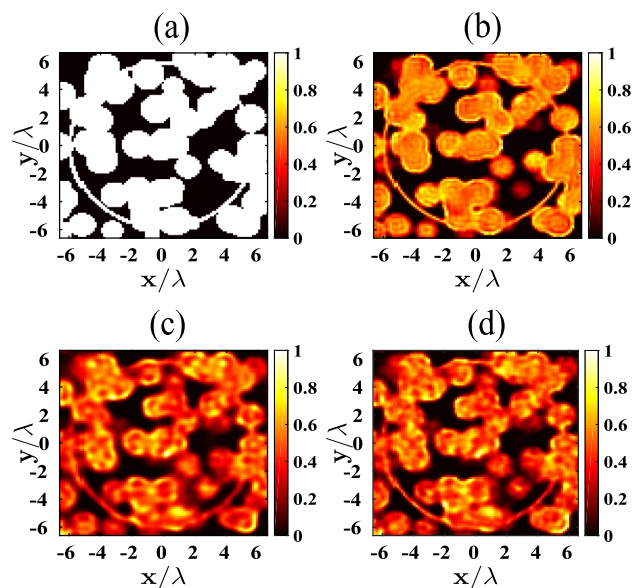

Fig. 4. Reconstruction of a fluorescent sample made of beads inside and outside two halves of a big sphere (mimicking a membrane). (a) Cut of the actual fluorescence distribution in the $y = 2.6\lambda$ plane. (b) Positive deconvolution of the confocal microscope image. (c) Positive deconvolution of the brightfield image. (d) Sample reconstruction with blind-SIM-SD. The blind-SIM approach yields an optical sectioning and axial resolution improvement approaching that of the confocal image. The colorbar indicates the normalized fluorescence density.

of the blind-SIM-SD approach as compared to brightfield fluorescence imaging. Except for the grainy aspect stemming from the residual inhomogeneity of the speckle averages, the blind-SIM reconstructions are roughly similar to that of the ideal confocal images and permit us to distinguish both the surface-like and the volumic objects.

Fig. 3. Reconstruction of a sample made of fluorescent thin (x–y) planes placed at different distances from the focal plane. (a) Cut of the actual fluorescence distribution in the $y = 0$ plane. (b) Positive deconvolution of the ideal confocal microscope image. (c) Positive deconvolution of the brightfield image. (d) Reconstruction with blind-SIM-SD. The blind-SIM approach yields an optical sectioning approaching that of the confocal image. The colorbar indicates the normalized fluorescence density.

Fig. 5. Same as Fig. 4, but the cut is done in the $z = -1.6\lambda$ plane. The blind-SIM approach yields a transverse resolution improvement comparable to that of the confocal image.

Up to now, the simulations were performed with an important global photon budget in order to check the behavior of the algorithms in an optimal configuration. In the last example, we consider the same sample as the one used in Figs. 4 and 5, but we reduce the global average photon budget per pixel to 10^4. This value corresponds to an average of 100 photons per pixel per speckle image. In this case, the Poisson noise is important as illustrated by the x–z cut of a non-noisy [Fig. 6(a)] and noisy [Fig. 6(b)] single speckle image. The brightfield image, obtained by adding the 100 speckle images, is displayed in Fig. 6(c), and its deconvolution is shown in Figs. 6(e) and 6(g). Figure 6(d) shows the positive deconvolution of the noisy single speckle image. Obviously, one cannot recover the fluorescent sample from just one single speckle image. However, when the 100 deconvolved speckle images are summed, see Figs. 6(f) and 6(h), the sample is recovered with a better resolution than that of the deconvolved brightfield image.

To complete the analysis of Blind-SIM-SD performances, we have conducted, on the star sample depicted in Fig. 2, a systematic study of the reconstruction accuracy with respect to the number of illuminations L and to the global photon budget. We define the error of the reconstructed fluorescence density $\hat{\rho}$ as

$$\mathrm{err}_\rho = \frac{\sum_{n=1}^{N} \|\hat{\rho}(\mathbf{r}_n) - \rho(\mathbf{r}_n)\|^2}{\sum_{n=1}^{N} \|\rho(\mathbf{r}_n)\|^2}. \tag{9}$$

Table 1 shows the influence of the number of illuminations on the reconstruction error. The photon budget per image pixel is taken equal to 10,000 so that the photon noise is negligible. We observe that the amelioration brought about by the increase of illuminations is significant up to 100 speckles but remains marginal beyond that limit. This behavior was to be expected as the standard deviation of the speckle average decreases slowly as $1/\sqrt{L}$.

Table 2 shows the role of the global photon budget on the reconstruction accuracy for $L = 100$ speckles. It is observed that, below 10,000 photons, the reconstruction is severely impacted by the photon noise. On the other hand, above 10,000 photons, the reconstruction error is mainly due to the speckle residual inhomogeneity. These results, in agreement with that of Fig. 6, confirm that blind-SIM-SD can be used in realistic microscopy experiments with a limited number of illuminations and a reasonable global photon budget.

4. CONCLUSION AND PERSPECTIVES

In conclusion, we have studied speckle illumination for three-dimensional high-resolution fluorescence microscopy (3D blind-SIM). By summing the deconvolution, under the positivity constraint, of each speckle image, we obtained an improved reconstruction of the sample fluorescence that compared favorably to that of an ideal confocal microscope. We believe that speckle blind-SIM can be an interesting alternative to confocal microscopy. Its major advantage is that it is a widefield technique without any control on the illuminations and there is no loss of photons in the detection scheme. Basically, one hundred speckles are enough to retrieve a satisfactory image. Its drawback is that it requires recording a 3D image for each speckle illumination. This task is delicate and,
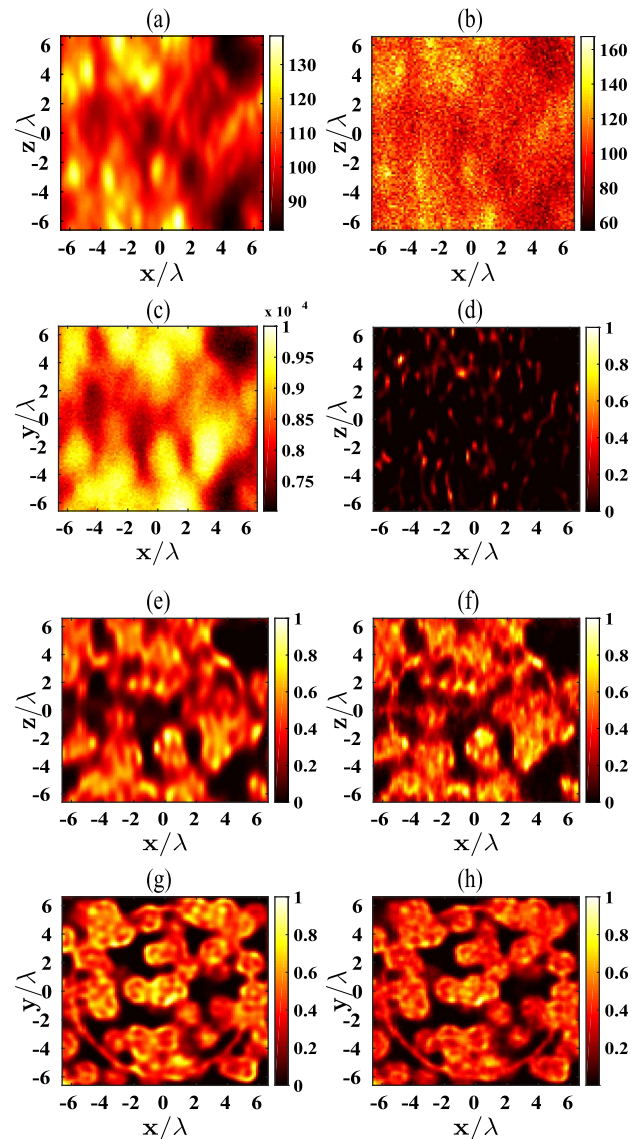
Fig. 6. Reconstructions of the same sample as that of Fig. (4) from data corrupted with realistic Poisson noise. (a) Single speckle image without noise in the $y = 2.6\lambda$ plane. (b) Same as (a), but the data are corrupted with Poisson noise. (c) Noisy brightfield image obtained by summing the 100 noisy speckle images. (d) Positive deconvolution of a single speckle image in the $y = 2.6\lambda$ plane. (e) Positive deconvolution of the brightfield image in the $y = 2.6\lambda$ plane. (f) Blind-SIM-SD reconstruction in the $y = 2.6\lambda$ plane. (g) Positive deconvolution of the brightfield image in the $z = -1.6\lambda$ plane. (h) Blind-SIM-SD reconstruction in the $z = -1.6\lambda$ plane. In (a), (b), and (c), the colorbar indicates the number of photons. In (d)–(h), the colorbar indicates the normalized fluorescence density.

Table 1. Reconstruction Error of the Star Sample Depicted in Fig. 2 Versus the Number of Illuminations^a

Number of speckles	200	100	50	20
err_ρ	0.186	0.202	0.266	0.313

^{a}Almost no photon noise.

Table 2. Reconstruction Error of the Star Sample Versus the Global Photon Budget[a]

Photon budget	10^6	10^5	10^4	5000
err_ρ	0.189	0.203	0.215	0.318

[a]The number of illuminations is taken as equal to $L = 100$.

in practice, should be done via remote focusing or by using a device projecting several foci planes on the camera in one shot [10].

APPENDIX A: ANALYSIS OF THE INVERSION PROCEDURE

In this appendix, we present the positive deconvolution that is used in the blind-SIM-SD algorithm. We consider one image M^{mes} obtained for a given illumination I which is modeled as

$$M^{\text{mes}} = \mathbf{A}(q), \tag{A1}$$

where $q = \rho I$, and ρ is the sample fluorescence density. We introduce the auxiliary function η such that $\eta^2 = q$ in order to enforce the positivity of the sought parameter q. The imaging problem is stated as finding q such that the cost functional $\mathcal{F}(\eta)$ is minimum,

$$\mathcal{F}(\eta) = \frac{1}{2} \|M^{\text{mes}} - \mathbf{A}(\eta^2)\|^2. \tag{A2}$$

This optimization problem is solved iteratively using a Polak–Ribière conjugate gradient method. A sequence (η_n) is built up according to the following recursive relation:

$$\eta_n = \eta_{n-1} + \alpha_n d_n, \tag{A3}$$

with η_n and η_{n-1} as estimations of η for the iteration step n and $n-1$, respectively. The function d_n represents the Polak–Ribière conjugate gradient direction

$$d_n = g_{\eta;n} + \gamma_n d_{n-1}, \tag{A4}$$

with

$$\gamma_n = \frac{\langle g_n | g_{\eta;n} - g_{\eta;n-1} \rangle}{\|g_{\eta;n}\|^2}. \tag{A5}$$

The function $g_{n,\eta}$ is the gradient of the cost functional $\mathcal{F}(\eta)$ with respect to η evaluated for the estimation η_{n-1}. This gradient reads as

$$g_{n,\eta} = -2\eta \mathbf{A}^\dagger(v_{n-1}), \tag{A6}$$

where $v_{n-1} = M^{\text{mes}} - \mathbf{A}(\eta_{n-1}^2)$ is the residual error at iteration $(n-1)$, and $\mathbf{A}^\dagger$ is the adjoint operator of $\mathbf{A}$, given by

$$\mathbf{A}^\dagger(u) = u * h^t, \tag{A7}$$

where h^t is the symmetric function of h. Once the updating direction is computed, the real scalar α_n is determined at each iteration step by minimizing the cost function as

$$\mathcal{F}(\alpha_n) = \frac{1}{2} \|M^{\text{mes}} - \mathbf{A}(\eta_n^2)\|^2$$
$$= \frac{1}{2} \|v_{n-1} - 2\alpha_n \mathbf{A}(\eta_n d_n) - \alpha_n^2 \mathbf{A}(d_n^2)\|^2. \tag{A8}$$

The minimization of this cost function, which is a polynomial in α of the fourth order, is achieved numerically using the Polak–Ribière conjugation gradient method [15]. In all the provided reconstructions, the initial estimate was a constant over the volume and the iterations were stopped when the cost functional reached a plateau.

REFERENCES

1. X. Hao, C. Kuang, Z. Gu, Y. Wang, S. Li, Y. Ku, Y. Li, J. Ge, and X. Liu, "From microscopy to nanoscopy via visible light," Light Sci. Appl. **2**, e108 (2013).
2. J. Mertz, "Optical sectioning microscopy with planar or structured illumination," Nat. Methods **8**, 811–819 (2011).
3. M. A. A. Neil, R. Juškaitis, and T. Wilson, "Method of obtaining optical sectioning by using structured light in a conventional microscope," Opt. Lett. **22**, 1905–1907 (1997).
4. D. Lim, T. N. Ford, K. K. Chu, and J. Mertz, "Optically sectioned *in vivo* imaging with speckle illumination HiLo microscopy," J. Biomed. Opt. **16**, 016014 (2011).
5. M. G. Gustafsson, L. Shao, P. M. Carlton, C. J. R. Wang, I. N. Golubovskaya, W. Z. Cande, D. A. Agard, and J. W. Sedat, "Three-dimensional resolution doubling in wide-field fluorescence microscopy by structured illumination," Biophys. J. **94**, 4957–4970 (2008).
6. E. Mudry, K. Belkebir, J. Girard, J. Savatier, E. L. Moal, C. Nicoletti, M. Allain, and A. Sentenac, "Structured illumination microscopy using unknown speckle patterns," Nat. Photonics **6**, 312–315 (2012).
7. D. Keum, S.-W. Ryu, C. Choi, K.-H. Jeong, J. Min, J. Jang, and J. C. Ye, "Fluorescent microscopy beyond diffraction limits using speckle illumination and joint support recovery," Sci. Rep. **3**, 2075 (2013).
8. M. Kim, C. Park, C. Rodriguez, Y. Park, and Y. H. Cho, "Superresolution imaging with optical fluctuation using speckle patterns illumination," Sci. Rep. **3**, 16525 (2015).
9. E. Botcherby, R. Juskaitis, M. Booth, and T. Wilson, "An optical technique for remote focusing in microscopy," Opt. Commun. **281**, 880–887 (2008).
10. S. Abrahamsson, J. Chen, B. Hajj, S. Stallinga, A. Y. Katsov, J. Wisniewski, G. Mizuguchi, P. Soule, F. Mueller, C. D. Darzacq, X. Darzacq, C. Wu, C. I. Bargmann, D. A. Agard, M. Dahan, and M. G. L. Gustafsson, "Fast multicolor 3D imaging using aberration-corrected multifocus microscopy," Nat. Methods **10**, 60–63 (2013).
11. R. Ayuk, H. Giovannini, A. Jost, E. Mudry, J. Girard, T. Mangeat, N. Sandeau, R. Heintzmann, K. Wicker, K. Belkebir, and A. Sentenac, "Structured illumination fluorescence microscopy with distorted excitations using a filtered blind-SIM algorithm," Opt. Lett. **38**, 4723–4726 (2013).
12. A. Jost, E. Tolstik, P. Feldmann, K. Wicker, A. Sentenac, and R. Heintzmann, "Optical sectioning and high resolution in single-slice structured illumination microscopy by thick slice blind-SIM reconstruction," PLoS ONE **10**, e0132174 (2015).
13. G. Cox and C. J. R. Sheppard, "Practical limits of resolution in confocal and nonlinear microscopy," Microsc. Res. Tech. **63**, 18–22 (2004).
14. R. Heintzmann, "Estimating missing information by maximum likelihood deconvolution," Micron **38**, 136–144 (2007), special issue on Super-resolution and Other Novel Microscopies.
15. W. H. Press, B. P. Flannery, S. A. Teukolski, and W. T. Vetterling, *Numerical Recipes* (Cambridge University, 1986).